Available online www.jsaer.com

***Journal of Scientific and Engineering Research*, 2018, 5(3):152-165**

Research Article

ISSN: 2394-2630
CODEN(USA): JSERBR

Fracture Pressure Prediction (FPP) from Well Log

Opiriyabo I. Horsfall*, Lawrence Idahosa, Onengiyeofori A. Davies

Department of Physics, Rivers State University, Port Harcourt. Nigeria

Abstract Qualitative study of fracture pressure prediction from composite well logs using Bower's and Eaton's methods have been carried out in order to identify hydrocarbon prospects, assessing the presence and quality of source rocks, building a structural and stratigraphic model from seismic data, provide right drilling mud weight and de-risking whether a particular play or basin should further be explored. Rock physics interpretational software ROKDOC was used to analyze the data set from the composite well logs and comparison with repeat formation tester (RFT) log data was established. The results showed that overpressure for well A and B was observed at depth below 7700ft, the formation pressure gradient ranges from 0.836psi/ft to 0.934psi/ft for well A and 0.830psi/ft to 0.928psi/ft and the fracture gradient from 0.790 psi/ft. The results of the present study would be useful in assessing seal effectiveness, mapping of hydrocarbon migration pathways, trap configuration, basin geometry, basin modelling, and safe and economic drilling.

Keywords Overpressure, Fracture Pressure, Disequilibrium, Pore Pressure Prediction

Introduction

Fracture pressure is the pressure in the wellbore at which a formation will crack, this is due to three principal stresses, the vertical stress σ_v, minimum and maximum horizontal stresses σ_H (Figure 1). The formation will fracture when the pressure in the wellbore exceeds the least of the stresses within the rock structure. Minimizing the risk associated with drilling wells is very important in today's oil and gas exploration and it is dependent on the understanding of the expected pressure regime to be encountered in the subsurface. Frequency of the formation fluid pressure above the pressure of a static column of water extending to the surface (termed overpressure) is a major concern in exploration and production of oil and gas. The prediction of an accurate fracture pressure will help to provide the right drilling mud weight. If it is too low, a blowout might occur and conversely, if it is too high, the formation might be damaged by invasion of the drilling fluid.

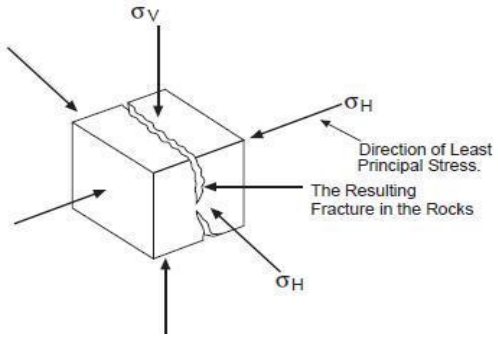

Figure 1: Diagram showing the three principal stresses in a formation

Most sedimentary basins exhibit overpressures [10, 14, 27], and as the industry explores for deeper targets, encountering high pressures becomes more common.

Overpressured formations are characterized by the following properties when compared with a normally pressured section at the same depth, higher porosities, lower bulk densities, lower effective stresses, higher temperatures lower interval velocities, higher Poisson's ratios and velocity reversals. [6, 25]

Overpressure poses a major threat to the success of exploration and production of hydrocarbon within oil fields in the Niger Delta oil field [13, 25]. Rapid processes of deposition and sedimentation that builds up tertiary basins have resulted into under-compaction at depths [19].

This fluid retention is most favoured by the presence of low permeability rocks such as shales, evaporates, and well cemented carbonates often referred to as seals. This seals prevent the escape of pore fluids at rates sufficient enough to compensate for the rate of increase in vertical stress induced by the overlying beds, and thus the pore fluid pressure begins to carry a large part of the load, and thereby increase the pore fluid pressure. Pressure compartments are characterized by their distinct pressure regimes which affect the maturation, migration and trapping history of hydrocarbons [14]. An understanding of the rock and fluid characteristics of the subsurface formation is of critical importance in the evolution of oil and gas fields. Figure 2. Diagram showing Relationship between pressure distributions and depth [20].

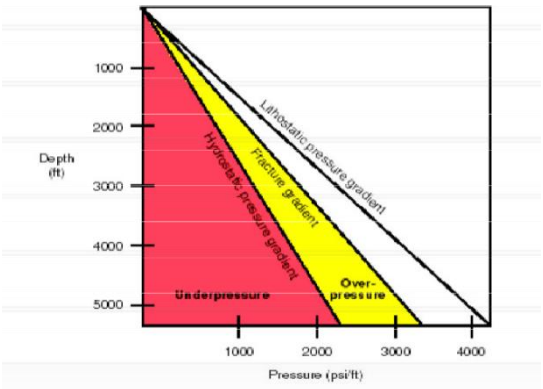

Figure 2: Relationship between pressure distributions and depth [20]

Geology of the Study Area

The study area falls within the Niger delta Basin of Nigeria. It lies between latitudes $3°N$ and $6°N$, and longitudes $5°E$ and $8°E$, in the Gulf of Guinea in Equitorial West Africa(Southern Nigeria), forming one of the World's most prolific hydrocarbon province. Extensive details of the Niger Delta was given by Figure 3. [21]. The Niger Delta basin is divided into mainly three lithostratigraphic units, the Akata (Palocene to Recent), Agbada (Eocene to Recent) and the Benin (Oligocene to Recent) Formations which conforms with a lower pro-delta lithofacies, a middle delta front lithofacies and an upper delta top facies respectively [1, 2]. These researchers have shown that the Akata Formation which comprised mainly of marine shale with sandy and silty beds laid down in turbidites and continental slope channel fills, about 7000 meters in thickness, serves as the source rock; Agbada Formation on the other hand which is over 3700 meters thick is the main hydrocarbon bearing unit consisting mainly of sandstone at the top with shaley intercalations and predominantly shale with sandstone intercalations at the lower part, finally the Benin Formation is about 2100 meters, and is composed of continental sands and gravels. It is the main ground water bearing formation in the Niger Delta Basin.

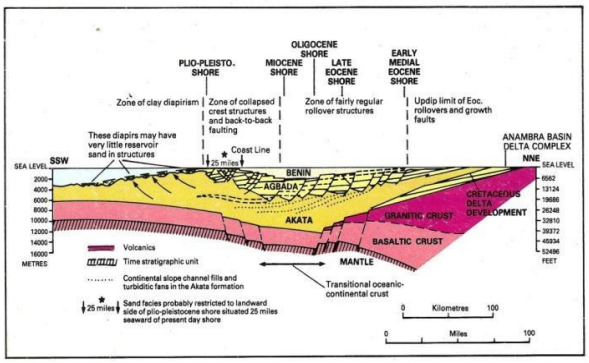

Figure 3: Akata, Agbada and Benin Formations [21]

Materials and Methods

Two Composite well Logs obtained from Shell Petroleum Development Company (SPDC) including Gamma Ray, Resistivity, Density, Sonic and Caliper Logs was used to actualize the aim of this work. Rock physics interpretational software ROKDOC was used to carry out the interpretation of the sourced data after an initial quality control checks were carried out on the data. Overburden stress and Shale Volume was determined using the gamma ray logs. Normal Compaction trend (NCT) of Shale and relationship between V_p-Rho crossplot was established [12]. Shales are preferred lithology for pore pressure interpretation. Overburden stress was generated for well A and B (Figure 7 and 8), NCT was generated for well A and B (Figure 9 and 10) and V_p-Rho crossplot for well A and B was carried out (Figure 11 and 12).

The volume of shale was calculated from the GR log using the equation:

$$V_{(sh)} = \frac{GR_{\log} - GR_{\min}}{(GR_{\max} - GR_{\min})} \quad (1)$$

Where V_{sh} = Volume of shale; GR_{log} = Gamma ray reading of formation; GR_{min} = Minimum Gamma ray (Clean sand); GR_{max} = Maximum gamma ray (Shale). The Volume of Sand was calculated using the equation: V_{sand} = 1–Vshale. A shale cut off of 0.65 was applied to the V_{shale} to make a lithologic discrimination between sand and shale sequence, such that interval with volume of shale less than 0.65 is classified as sand and intervals with Volume of shale greater than 0.65 is grouped as shale.

Since pressures are predicted in shale, the velocity reading within the clean shale intervals were picked out (termed Vp shale trend), from which the normal compaction trend is established.

The observed velocity in shale (Vp shale trend) and the velocity of a normally compacted shale (the result of fitting a line of best fit to the shallow section assumed to be normally compacted) are inputs in Eaton model equation. Using Rho log, the bulk density log is used in the calculation of the overburden stress. Repeat Formation Tester (RFT) data are measured data at reservoir intervals to which the results of the prediction are compared. RFT points were represented as a green triangle on the pressure view interface (Figure 13 and 14), which serves as landmark markers confirming the accuracy or not of our prediction. If the predictions calibrate well with the RFT points, it is an indication that the results of the prediction at other points where there is no RFT data can be trusted.

Acoustic sonic velocity is inputted into the equation of the methods using ROKDOC to establish the relationship. It is crucial to establish a relationship between velocities and pore pressure using offset well data. This is to enable us to test how reliably well, the acoustic parameter can be used to determine the formation pressure and to as well derive the calibration parameters required in the methods used. The accuracy of the relationship is based on the availability of measured pressure data to logged depth, which serves as a calibrating standard.

Equation 2 is the founding equation based on [23] Soil mechanics experiment upon which the two models; The Bowers and Eaton's model [4, 7].

A derivation Eaton and Bowers relationship from Terzhagi relationship is as shown:

$$\sigma = S - P \quad (2)$$

EATONS MODEL

$$\sigma = \sigma_N \left(\frac{v}{v_n}\right)^3 \quad (3)$$

$$P_p = (S_v - P_n)\left(\frac{\Delta V_{P_{obs}}}{\Delta V_{P_{norm}}}\right)^3 \quad (4)$$

Then

BOWERS MODEL

$$V_p = V_{ml} + A\sigma_e^{\ B} \quad (5)$$

$$\sigma = \left(\frac{V_p - V_{ml}}{A} \right)^{\frac{1}{B}} \quad (6)$$

$$P_p = S_v - \left(\frac{V_p - V_{ml}}{A} \right)^{\frac{1}{B}} \quad (7)$$

where: σ = effective stress; S = overburden stress; P = pore pressure; σ_n = Effective Stress of a normal compaction; v_n = Velocity of normally compacted formation, v = Observed velocity; Pp = formation pore pressure gradient; P_n = hydrostatic pore pressure gradient (normally 0.45 psi/ft or 1.03Mpa/km, dependent on water gradient salinity); Vp_{obs} = velocity observed; Vp_{norm} = velocity on normal trend; Vp = the compressional velocity at a given depth; V_{ml} = the compressional velocity in the mudline (i.e. the sea floor or the ground surface); A and B are the parameters calibrated with offset velocity versus effective stress; σ_e= effective stress.
The result of Eaton equation and Bowers equation was called Eaton model and Bowers model in the final prediction. This was achieved by putting the various parameters in the equation for each well and the results was plotted against depth to get the blue line and the red line termed Bowers and Eaton model.

Fracture Pressure Prediction

The detected pore pressure was applied in the equation of fracture pressure prediction to determine the minimum stress at which a formation will fracture [16].

$$F_p = K (Sv - P_p) + P_p \quad (8)$$

Where Sv = Lithostatic stress; P_p = Pore Pressure; K = Stress ratio; F_p = Fracture pressure. The fracture pressure is the black line in
Fracture pressure is the pressure in the wellbore at which a formation will crack
The pressure at which formations will fracture when exposed to borehole pressure is determined by conducting Leak-off test

Leak off Test (LOTs)

Estimates of minimum stress from leak off tests (LOTs)
LOTs are performed to assess the minimum stress values in the section cut by the wellbore. The LOT is generally conducted after casing has been set in the well and cement has been applied to isolate the shallower sections from any higher pressure fluids that may be encountered deeper in the section.
Firstly, a short section (typically 20 feet) is drilled below the base of the cement before increasing the pressure in the borehole until mud is lost into the formation. The pressure in the mud is continuously monitored and recorded throughout the test. As long as the cement is sound, mud loss is a consequence of failure of the rock usually by the propagation of fractures in the direction of minimum stress. The LOT pressure value represents the magnitude of the minimum stress plus the tensile strength of the formation, which has to be exceeded before fractures will form [17].
In many cases "leak off " is not reached, but a defined maximum pressure is reached without mud loss, and considered high enough to continue drilling ahead safely. This is often referred to as a formation integrity test [22].

Results and Discussion

Fracture pore pressure data derived from the two wells are presented in tables 1 and 2. These pressure data was plotted against depth for the two wells , and the results is presented in figures (4 and 5).the results from the plots showed that fracture pressure increases with an increasing depth, this is due to the increasing overburden(rock layers) pressure. The well logs A and B used for the study is also presented. (Figure 6 and 7). From Figure 8 and 9 for well A and B, the grey line on the right represent overburden pressure of a fixed gradient, while the black line is the estimated overburden gradient from density log with the error margin in dotted line. To the left hand side is the density log (Rho) and the Rho fit. The detection of overpressures was done by generating sonic

velocities from Non compaction trend (NCT) and crossplotting of the velocities with density with the aid of colour code indices. This is shown in figures 10, 11, 12 and 13.Velocity–density crossplot for the wells showed a typical compaction disequilibrium curve for both Well A and B indicated that there is an increase in density with a corresponding increase in velocity at depth 8000ft.

The lithology derived from gamma ray log GR log showed a typical sand dominated Benin Formation to a depth of about 7,500 ft. in both Wells A and B. The overburden gradient derived from the density log from (Figures 8, and 9) plotted parallel to the line of a fixed gradient of 1.0 psi/ft. and it ranges from 0.836 psi/ft. to 0.934 psi/ft. for Well A, and 0.830 psi/ft. to 0.928 psi/ft. for Well B. The grey line on the right represent overburden pressure of a fixed gradient, while the black line is the estimated overburden gradient from density log with the error margin in dotted line. The left hand is the density log (Rho) and the Rho fit. The onset of overpressure was observed at 7,700 ft for both wells which corresponds to the first Agbada shale Formation. Bowers loading model and Eaton model used for detection of overpressure at the interval shown to have undergone compaction disequilibrium gave a good match with the measured pressures where available. The result of the prediction showed that pressure gradient in Well A and B increased from hydrostatic pressure gradient (0.433 psi/ft.) to about 0.6 psi/ft. (mild over pressured), the fracture pressure prediction using Matthew and Kelliy equation estimated a fracture gradient from 0.790psi/ft for well A and B (Figure 14 and 15), represents the final prediction of pressure-depth profile of Well A and Well B.

Table 1: Fracture Pore Pressure Data for Well A

TVDml	FPP	TVDml	FPP	TVDml	FPP
7700.31	6084.745	7721.81	6090.602	7743.31	6101.41
7700.81	6084.828	7722.31	6090.795	7743.81	6101.731
7701.31	6084.912	7722.81	6090.992	7744.31	6102.055
7701.81	6084.996	7723.31	6091.196	7744.81	6102.381
7702.31	6085.082	7723.81	6091.406	7745.31	6102.712
7702.81	6085.175	7724.31	6091.623	7745.81	6103.048
7703.31	6085.276	7724.81	6091.844	7746.31	6103.388
7703.81	6085.383	7725.31	6092.066	7746.81	6103.73
7704.31	6085.491	7725.81	6092.29	7747.31	6104.076
7704.81	6085.599	7726.31	6092.511	7747.81	6104.424
7705.31	6085.708	7726.81	6092.73	7748.31	6104.775
7705.81	6085.819	7727.31	6092.949	7748.81	6105.127
7706.31	6085.933	7727.81	6093.17	7749.31	6105.48
7706.81	6086.049	7728.31	6093.395	7749.81	6105.835
7707.31	6086.166	7728.81	6093.622	7750.31	6106.192
7707.81	6086.282	7729.31	6093.848	7750.81	6106.555
7708.31	6086.4	7729.81	6094.075	7751.31	6106.921
7708.81	6086.522	7730.31	6094.305	7751.81	6107.292
7709.31	6086.647	7730.81	6094.539	7752.31	6107.668
7709.81	6086.774	7731.31	6094.776	7752.81	6108.05
7710.31	6086.905	7731.81	6095.016	7753.31	6108.439
7710.81	6087.04	7732.31	6095.259	7753.81	6108.831
7711.31	6087.177	7732.81	6095.504	7754.31	6109.224
7711.81	6087.315	7733.31	6095.751	7754.81	6109.619
7712.31	6087.453	7733.81	6096.001	7755.31	6110.019
7712.81	6087.594	7734.31	6096.255	7755.81	6110.424
7713.31	6087.74	7734.81	6096.513	7756.31	6110.834
7713.81	6087.891	7735.31	6096.775	7756.81	6111.25
7714.31	6088.047	7735.81	6097.038	7757.31	6111.673
7714.81	6088.205	7736.31	6097.304	7757.81	6112.102
7715.31	6088.364	7736.81	6097.575	7758.31	6112.537

7715.81	6088.525	7737.31	6097.851	7758.81	6112.976
7716.31	6088.688	7737.81	6098.129	7759.31	6113.418
7716.81	6088.853	7738.31	6098.41	7759.81	6113.86
7717.31	6089.018	7738.81	6098.691	7760.31	6114.301
7717.81	6089.184	7739.31	6098.976	7760.81	6114.741
7718.31	6089.353	7739.81	6099.264	7761.31	6115.181
7718.81	6089.525	7740.31	6099.558	7761.81	6115.622
7719.31	6089.699	7740.81	6099.858	7762.31	6116.066
7719.81	6089.874	7741.31	6100.162	7762.81	6116.511
7720.31	6090.052	7741.81	6100.469	7763.31	6116.961
7720.81	6090.232	7742.31	6100.778	7763.81	6117.416
7721.31	6090.415	7742.81	6101.092	7764.31	6117.874
7764.81	6118.337	7786.31	6141.46	7807.81	6162.262
7765.31	6118.806	7786.81	6141.911	7808.31	6163.074
7765.81	6119.28	7787.31	6142.363	7808.81	6163.879
7766.31	6119.76	7787.81	6142.813	7809.31	6164.68
7766.81	6120.25	7788.31	6143.254	7809.81	6165.477
7767.31	6120.747	7788.81	6143.681	7810.31	6166.27
7767.81	6121.251	7789.31	6144.093	7810.81	6167.06
7768.31	6121.763	7789.81	6144.494	7811.31	6167.848
7768.81	6122.289	7790.31	6144.883	7811.81	6168.633
7769.31	6122.827	7790.81	6145.261	7812.31	6169.417
7769.81	6123.367	7791.31	6145.633	7812.81	6170.205
7770.31	6123.905	7791.81	6146	7813.31	6170.998
7770.81	6124.437	7792.31	6146.361	7813.81	6171.797
7771.31	6124.965	7792.81	6146.709	7814.31	6172.603
7771.81	6125.493	7793.31	6147.039	7814.81	6173.418
7772.31	6126.027	7793.81	6147.353	7815.31	6174.239
7772.81	6126.567	7794.31	6147.651	7815.81	6175.063
7773.31	6127.112	7794.81	6147.93	7816.31	6175.886
7773.81	6127.662	7795.31	6148.188	7816.81	6176.708
7774.31	6128.214	7795.81	6148.434	7817.31	6177.539
7774.81	6128.767	7796.31	6148.683	7817.81	6178.383
7775.31	6129.32	7796.81	6148.951	7818.31	6179.243
7775.81	6129.877	7797.31	6149.252	7818.81	6180.112
7776.31	6130.439	7797.81	6149.576	7819.31	6180.987
7776.81	6131.007	7798.31	6149.903	7819.81	6181.868
7777.31	6131.582	7798.81	6150.227	7820.31	6182.751
7777.81	6132.167	7799.31	6150.557	7820.81	6183.638
7778.31	6132.764	7799.81	6150.904	7821.31	6184.53
7778.81	6133.375	7800.31	6151.282	7821.81	6185.424
7779.31	6134.008	7800.81	6151.718	7822.31	6186.319
7779.81	6134.644	7801.31	6152.232	7822.81	6187.21
7780.31	6135.256	7801.81	6152.838	7823.31	6188.095
7780.81	6135.838	7802.31	6153.441	7823.81	6188.979
7781.31	6136.4	7802.81	6154.05	7824.31	6189.867
7781.81	6136.95	7803.31	6154.779	7824.81	6190.76
7782.31	6137.497	7803.81	6155.591	7825.31	6191.66
7782.81	6138.037	7804.31	6156.423	7825.81	6192.566
7783.31	6138.569	7804.81	6157.263	7826.31	6193.478

7783.81	6139.09	7805.31	6158.102	7826.81	6194.397
7784.31	6139.596	7805.81	6158.94	7827.31	6195.322
7784.81	6140.081	7806.31	6159.778	7827.81	6196.256
7785.31	6140.549	7806.81	6160.613	7828.31	6197.203
7785.81	6141.007	7807.31	6161.442	7828.81	6198.162

Table 2: Fracture Pore Pressure Data for Well B

TVDml	FPP	TVDml	FPP	TVDml	FPP	TVDml	FPP
7606.03	5988.17	7629.03	6012.26	7652.53	6039.79	7676.03	6071.67
7606.53	5988.88	7629.53	6012.88	7653.03	6040.33	7676.53	6072.44
7607.03	5989.6	7630.03	6013.51	7653.53	6040.88	7677.03	6073.22
7607.53	5990.32	7630.53	6014.17	7654.03	6041.43	7677.53	6074
7608.03	5991.04	7631.03	6014.84	7654.53	6042	7678.03	6074.78
7608.53	5991.76	7631.53	6015.53	7655.03	6042.58	7678.53	6075.57
7609.03	5992.47	7632.03	6016.23	7655.53	6043.16	7679.03	6076.35
7609.53	5993.14	7632.53	6016.92	7656.03	6043.75	7679.53	6077.15
7610.03	5993.78	7633.03	6017.61	7656.53	6044.35	7680.03	6077.94
7610.53	5994.4	7633.53	6018.3	7657.03	6044.95	7680.53	6078.75
7611.03	5995	7634.03	6018.99	7657.53	6045.56	7681.03	6079.56
7611.53	5995.58	7634.53	6019.69	7658.03	6046.18	7681.53	6080.37
7612.03	5996.14	7635.03	6020.39	7658.53	6046.81	7682.03	6081.17
7612.53	5996.68	7635.53	6021.07	7659.03	6047.43	7682.53	6081.98
7613.03	5997.2	7636.03	6021.75	7659.53	6048.07	7683.03	6082.78
7613.53	5997.72	7636.53	6022.42	7660.03	6048.7	7683.53	6083.59
7614.03	5998.21	7637.03	6023.08	7660.53	6049.35	7684.03	6084.4
7614.53	5998.7	7637.53	6023.74	7661.03	6050	7684.53	6085.21
7615.03	5999.17	7638.03	6024.39	7661.53	6050.66	7685.03	6086.02
7615.53	5999.63	7638.53	6025.02	7662.03	6051.32	7685.53	6086.82
7616.03	6000.09	7639.03	6025.63	7662.53	6051.99	7686.03	6087.63
7616.53	6000.54	7639.53	6026.23	7663.03	6052.66	7686.53	6088.44
7617.03	6000.98	7640.03	6026.82	7663.53	6053.34	7687.03	6089.25
7616.53	6001.42	7640.53	6027.4	7664.03	6054.03	7687.53	6090.07
7618.03	6001.85	7641.03	6027.97	7664.53	6054.72	7688.03	6090.89
7652.03	6002.28	7641.53	6028.54	7665.03	6055.41	7688.53	6091.7
7619.03	6002.7	7642.03	6029.09	7665.53	6056.11	7689.03	6092.52
7619.53	6003.13	7642.53	6029.64	7666.03	6056.82	7689.53	6093.34
7620.03	6003.56	7643.03	6030.17	7666.53	6057.52	7690.03	6094.17
7620.53	6003.99	7643.53	6030.7	7667.03	6058.23	7690.53	6095
7621.03	6004.42	7644.03	6031.22	7667.53	6058.95	7691.03	6095.83
7722.53	6004.84	7644.53	6031.73	7668.03	6059.66	7691.53	6096.67
7622.03	6005.27	7645.03	6032.23	7668.53	6060.39	7692.03	6097.5
7622.53	6005.71	7645.53	6032.73	7669.03	6061.11	7692.53	6098.34
7623.03	6006.15	7646.03	6033.22	7669.53	6061.84	7693.03	6099.18
7623.53	6006.6	7646.53	6033.69	7670.03	6062.58	7693.53	6100.02
7624.03	6007.05	7647.03	6034.16	7670.53	6063.32	7694.03	6100.86
7624.53	6007.51	7647.53	6034.63	7671.03	6064.07	7694.53	6101.69
7625.03	6007.98	7648.03	6035.11	7671.53	6064.81	7695.03	6102.52
7625.53	6008.46	7648.53	6035.61	7672.03	6065.56	7695.53	6103.34
7626.03	6008.95	7649.03	6036.11	7672.53	6066.31	7696.03	6104.17
7626.53	6009.46	7649.53	6036.62	7673.03	6067.06	7696.53	6105
7627.03	6009.99	7650.03	6037.13	7673.53	6067.82	7697.03	6105.83

7627.53	6010.52	7650.53	6037.65	7674.03	6068.59	7697.53	6106.67
7628.03	6011.08	7651.03	6038.18	7674.53	6069.35	7698.03	6107.51
7628.53	6011.66	7651.53	6038.71	7675.03	6070.12	7698.53	6108.34
7816.53	6265.12	7841.03	6263.83	7864.53	6275.2	11676.03	9568.09
7817.03	6265.24	11629.03	9472.61	11652.53	9518.02	11676.53	9569.18
7817.53	6265.35	11629.53	9473.52	11653.03	9519.04	11677.03	9570.27
11605.03	9434	11630.03	9474.43	11653.53	9520.07	11677.53	9571.37
11605.53	9434.71	11630.53	9475.33	11654.03	9521.11	11678.03	9572.47
11606.03	9435.42	11631.03	9476.24	11654.53	9522.13	11678.53	9573.59
11606.53	9436.14	11631.53	9477.14	11655.03	9523.16	11679.03	9574.7
11607.03	9436.86	11632.03	9478.05	11655.53	9524.18	11679.53	9575.82
11607.53	9437.59	11632.53	9478.97	11656.03	9525.2	11680.03	9576.93
11608.03	9438.32	11633.03	9479.89	11656.53	9526.23	11680.53	9578.04
11608.53	9439.06	11633.53	9480.83	11657.03	9527.26	11681.03	9579.14
11609.03	9439.8	11634.03	9481.77	11657.53	9528.3	11681.53	9580.24
11609.53	9440.54	11634.53	9482.72	11658.03	9529.36	11682.03	9581.34
11610.03	9441.28	11635.03	9483.66	11658.53	9530.43	11682.53	9582.45
11610.53	9442.02	11635.53	9484.61	11659.03	9531.49	11683.03	9583.57
11611.03	9442.77	11636.03	9485.56	11659.53	9532.56	11683.53	9584.68
11611.53	9443.51	11636.53	9486.5	11660.03	9533.62	11684.03	9585.78
11612.03	9444.27	11637.03	9487.46	11660.53	9534.68	11684.53	9586.89
11612.53	9445.03	11637.53	9488.42	11661.03	9535.73	11685.03	9588
11613.03	9445.79	11638.03	9489.38	11661.53	9536.78	11685.53	9589.11
11613.53	9446.56	11638.53	9490.36	11662.03	9537.82	11686.03	9590.22
11614.03	9447.34	11639.03	9491.33	11662.53	9538.87	11686.53	9591.33
11614.53	9448.13	11639.53	9492.3	11663.03	9539.92	11687.03	9592.44
11615.03	9448.92	11640.03	9493.27	11663.53	9540.97	11687.53	9593.56
11615.53	9449.71	11640.53	9494.23	11664.03	9542.02	11688.03	9594.67
11616.03	9450.51	11641.03	9495.18	11664.53	9543.07	11688.53	9595.78
11616.53	9451.31	11641.53	9496.14	11665.03	9544.14	11689.03	9596.9
11617.03	9452.11	11642.03	9497.1	11665.53	9545.21	11689.53	9598.02
11617.53	9452.92	11642.53	9498.07	11666.03	9546.28	11690.03	9599.13
11618.03	9453.74	11643.03	9499.04	11666.53	9547.36	11690.53	9600.25
11618.53	9454.56	11643.53	9500.01	11667.03	9548.44	11691.03	9601.36
11619.03	9455.39	11644.03	9500.98	11667.53	9549.52	11691.53	9602.48
11619.53	9456.21	11644.53	9501.96	11668.03	9550.61	11692.03	9603.6
11620.03	9457.04	11645.03	9502.94	11668.53	9551.72	11692.53	9604.72
11620.53	9457.87	11645.53	9503.93	11669.03	9552.82	11693.03	9605.85
11621.03	9458.7	11646.03	9504.92	11669.53	9553.93	11693.53	9606.97
11621.53	9459.53	11646.53	9505.92	11670.03	9555.03	11694.03	9608.09
11622.03	9460.36	11647.03	9506.91	11670.53	9556.13	11694.53	9609.21
11622.53	9461.2	11647.53	9507.91	11671.03	9557.23	11695.03	9610.33
11623.03	9462.04	11648.03	9508.92	11671.53	9558.32	11695.53	9611.45
11623.53	9462.88	11648.53	9509.93	11672.03	9559.4	11696.03	9612.57
11624.03	9463.74	11649.03	9510.93	11672.53	9560.47	11696.53	9613.69
11624.53	9464.59	11649.53	9511.93	11673.03	9561.55	11697.03	9614.81
11625.03	9465.46	11650.03	9512.94	11673.53	9562.63	11697.53	9615.93
11625.53	9466.34	11650.53	9513.94	11674.03	9563.71	11698.03	9617.03
11626.03	9467.22	11651.03	9514.96	11674.53	9564.8	11698.53	9618.12
11626.53	9468.12	11651.53	9515.97	11675.03	9565.9	11699.03	9619.21

11627.03	9469.03	11652.03	9516.99	11675.53	9567	12176.03	10606.43
11627.53	9469.93	12129.03	10516.73	12152.53	10566.48	12176.53	10607
11628.03	9470.82	12129.53	10517.73	12153.03	10567.56	12177.03	10607.55
11628.53	9471.71	12130.03	10518.74	12153.53	10568.63	12177.53	10608.08
12105.03	10465.52	12130.53	10519.75	12154.03	10569.69	12178.03	10608.61
12105.53	10466.59	12131.03	10520.75	12154.53	10570.74	12178.53	10609.13
12106.03	10467.66	12131.53	10521.74	12155.03	10571.79	12179.03	10609.64
12106.53	10468.72	12132.03	10522.74	12155.53	10572.83	12179.53	10610.15
12107.03	10469.79	12132.53	10523.72	12156.03	10573.87	12180.03	10610.64
12107.53	10470.85	12133.03	10524.71	12156.53	10574.89	12180.53	10611.11
12108.03	10471.92	12133.53	10525.7	12157.03	10575.91	12181.03	10611.57
12108.53	10472.99	12134.03	10526.68	12157.53	10576.92	12181.53	10612.01
12109.03	10474.07	12134.53	10527.68	12158.03	10577.92	12182.03	10612.43
12109.53	10475.15	12135.03	10528.67	12158.53	10578.91	12182.53	10612.85
12110.03	10476.24	12135.53	10529.67	12159.03	10579.89	12183.03	10613.26
12110.53	10477.34	12136.03	10530.67	12159.53	10580.86	12183.53	10613.65
12111.03	10478.44	12136.53	10531.68	12160.03	10581.81	12184.03	10614.02
12111.53	10479.55	12137.03	10532.69	12160.53	10582.75	12184.53	10614.38
12112.03	10480.65	12137.53	10533.72	12161.03	10583.68	12185.03	10614.72
12112.53	10481.76	12138.03	10534.76	12161.53	10584.6	12185.53	10615.05
12113.03	10482.86	12138.53	10535.8	12162.03	10585.5	12186.03	10615.36
12113.53	10483.97	12139.03	10536.85	12162.53	10586.4	12186.53	10615.66
12114.03	10485.07	12139.53	10537.91	12163.03	10587.29	12187.03	10615.94
12114.53	10486.17	12140.03	10538.98	12163.53	10588.16	12187.53	10616.2
12115.03	10487.26	12140.53	10540.06	12164.03	10589.02	12188.03	10616.46
12115.53	10488.36	12141.03	10541.15	12164.53	10589.87	12188.53	10616.71
12116.03	10489.46	12141.53	10542.24	12165.03	10590.71	12189.03	10616.95
12116.53	10490.55	12142.03	10543.33	12165.53	10591.54	12189.53	10617.19
12117.03	10491.65	12142.53	10544.42	12166.03	10592.36	12190.03	10617.42
12117.53	10492.74	12143.03	10545.51	12166.53	10593.17	12190.53	10617.64
12118.03	10493.83	12143.53	10546.61	12167.03	10593.97	12191.03	10617.86
12118.53	10494.91	12144.03	10547.71	12167.53	10594.76	12191.53	10618.07
12119.03	10495.99	12144.53	10548.81	12168.03	10595.54	12192.03	10618.26
12119.53	10497.06	12145.03	10549.92	12168.53	10596.31	12192.53	10618.45
12120.03	10498.13	12145.53	10551.03	12169.03	10597.07	12193.03	10618.63
12120.53	10499.2	12146.03	10552.15	12169.53	10597.82	12193.53	10618.81
12121.03	10500.26	12146.53	10553.26	12170.03	10598.55	12194.03	10618.98
12121.53	10501.32	12147.03	10554.38	12170.53	10599.26	12194.53	10619.14
12122.03	10502.37	12147.53	10555.5	12171.03	10599.97	12195.03	10619.29
12122.53	10503.42	12148.03	10556.61	12171.53	10600.67	12195.53	10619.43
12123.03	10504.47	12148.53	10557.73	12172.03	10601.36	12196.03	10619.56
12123.53	10505.51	12149.03	10558.84	12172.53	10602.04	12196.53	10619.68
12124.03	10506.55	12149.53	10559.95	12173.03	10602.71	12197.03	10619.79
12124.53	10507.59	12150.03	10561.05	12173.53	10603.36	12197.53	10619.88
12125.03	10508.62	12150.53	10562.14	12174.03	10604.01	12198.03	10619.97
12125.53	10509.64	12151.03	10563.23	12174.53	10604.64	12198.53	10620.05
12126.03	10510.67	12151.53	10564.32	12175.03	10605.25	12199.03	10620.13
12126.53	10511.69	12152.03	10565.41	12175.53	10605.85	12610.03	10877.82
12127.03	10512.71	12619.53	10887.86	12615.03	10883.08	12610.53	10878.35
12127.53	10513.72	12620.03	10888.39	12615.53	10883.61	12611.03	10878.87

12128.03	10514.73	12620.53	10888.92	12616.03	10884.14	12611.53	10879.39
12128.53	10515.73	12621.03	10889.45	12616.53	10884.67	12612.03	10879.92
12605.03	10872.66	12621.53	10889.98	12617.03	10885.2	12612.53	10880.44
12605.53	10873.18	12622.03	10890.52	12617.53	10885.74	12613.03	10880.96
12606.03	10873.69	12622.53	10891.05	12618.03	10886.27	12613.53	10881.49
12606.53	10874.21	12623.03	10891.59	12618.53	10886.8	12614.03	10882.02
12607.03	10874.72	12623.53	10892.13	12619.03	10887.33	12614.53	10882.55
12607.53	10875.24	12624.03	10892.67				
12608.03	10875.75	12624.53	10893.2				
12608.53	10876.27	12625.03	10893.74				
12609.03	10876.78	12625.53					
12609.53	10877.3	12626.03					

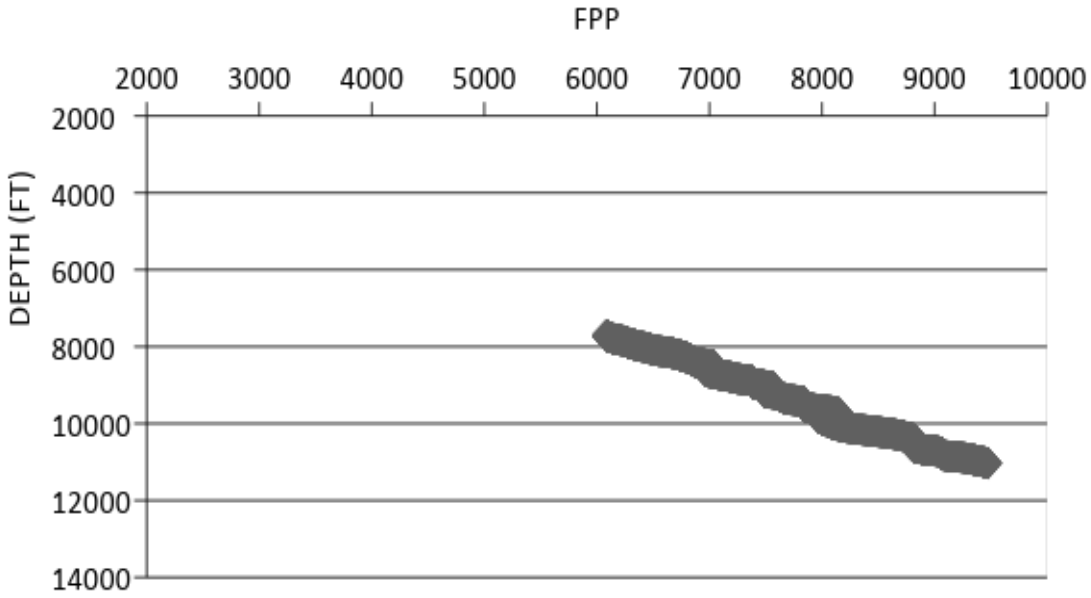

Figure 4: Plot of Pressure against Depth for well A

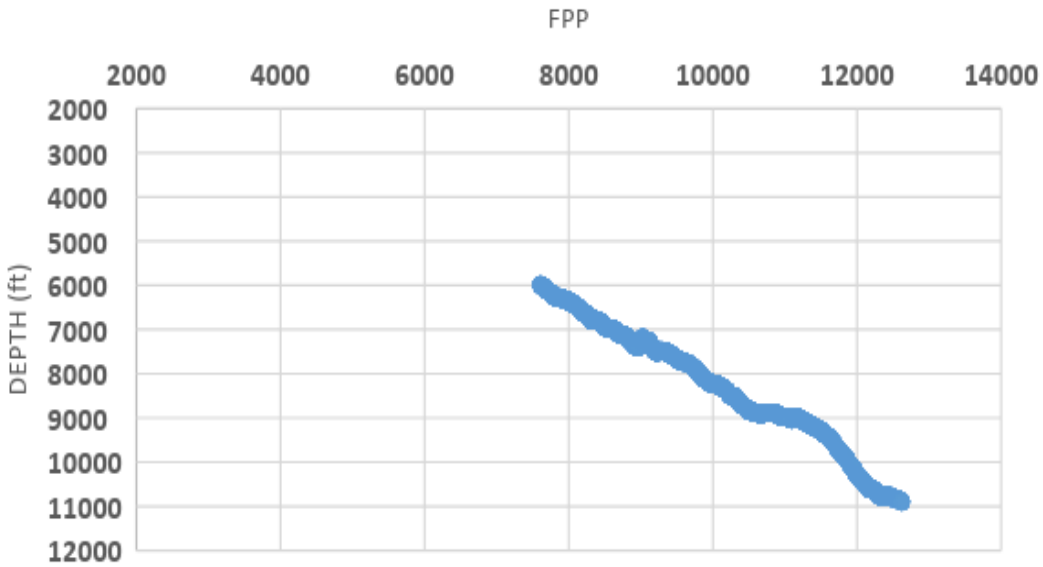

Figure 5: Plot of Pressure against Depth for well B

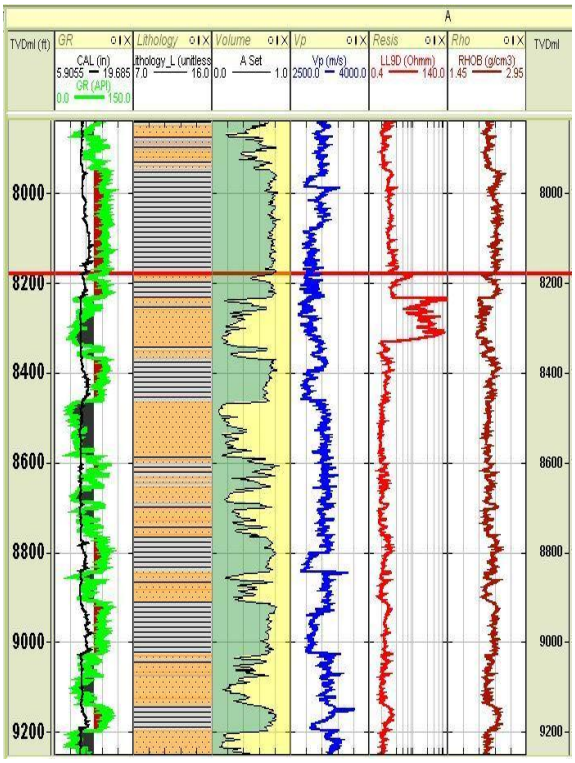

Figure 6: Well Log A.

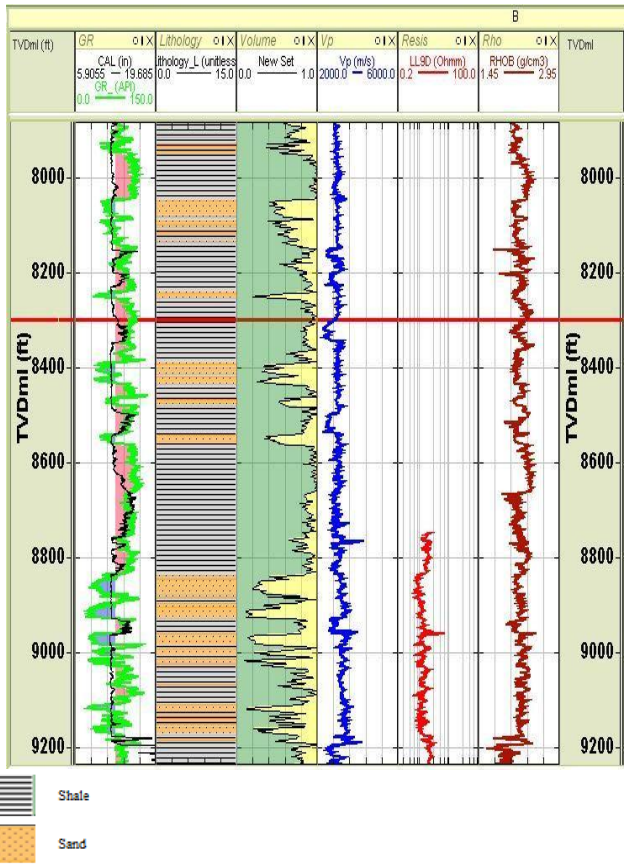

Figure 7:Well Log B

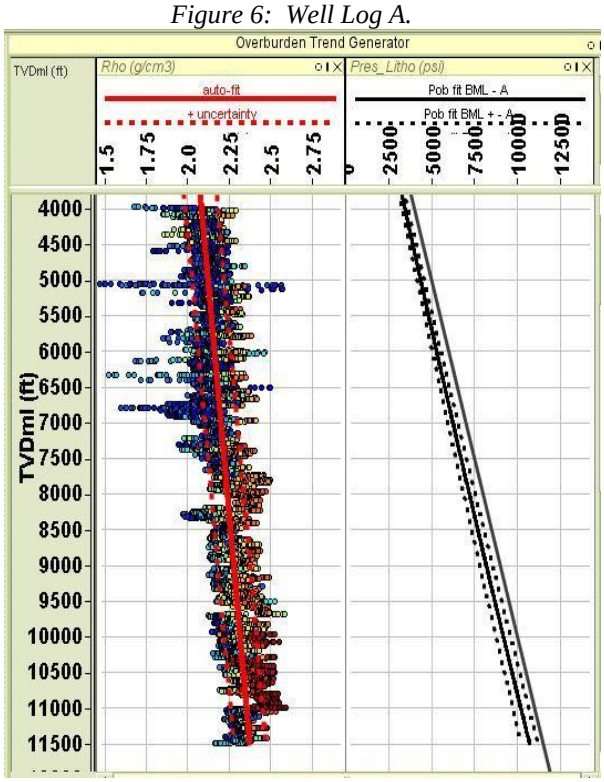

Figure 8: Well A, Sample of Overburden stress generated from density log.

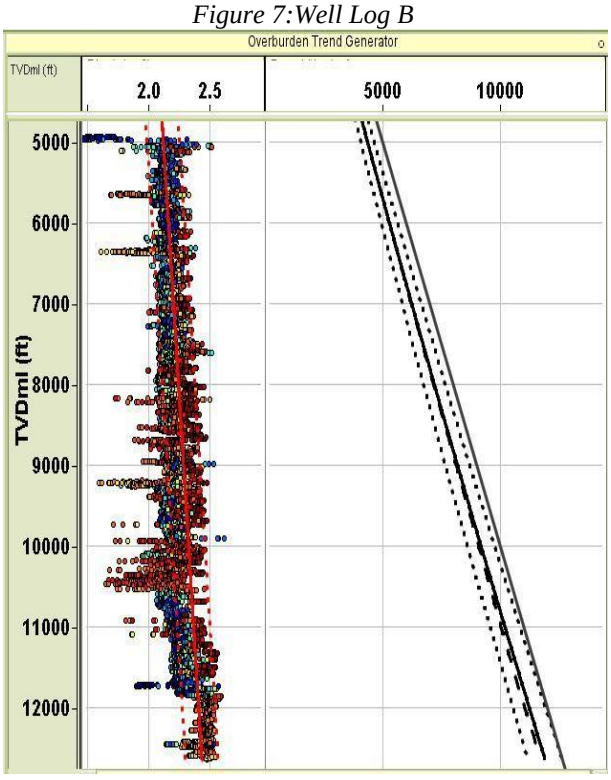

Figure 9: Well B, Sample of OVB Generated from the Density Log

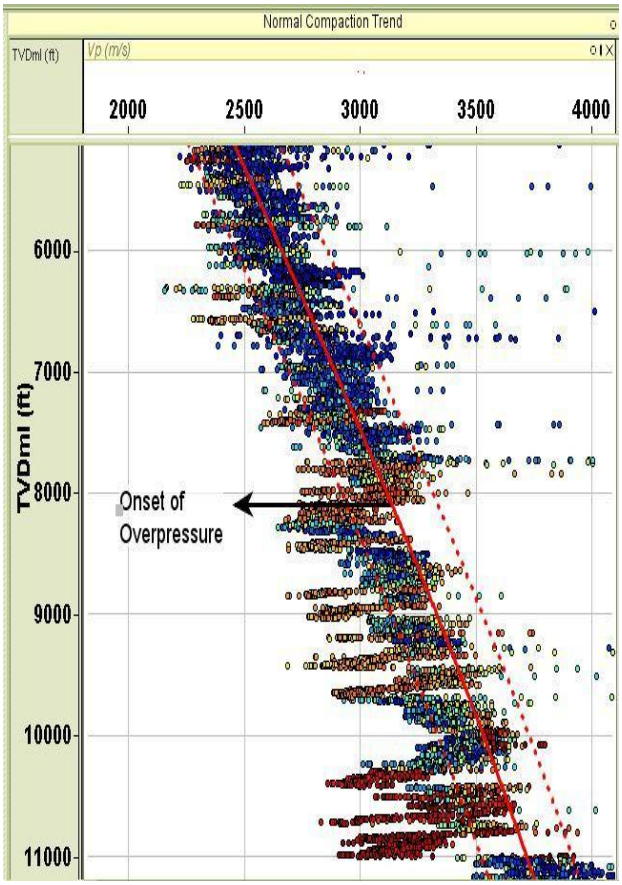

Figure 10: Showing sonic velocity generated NCT for Well A

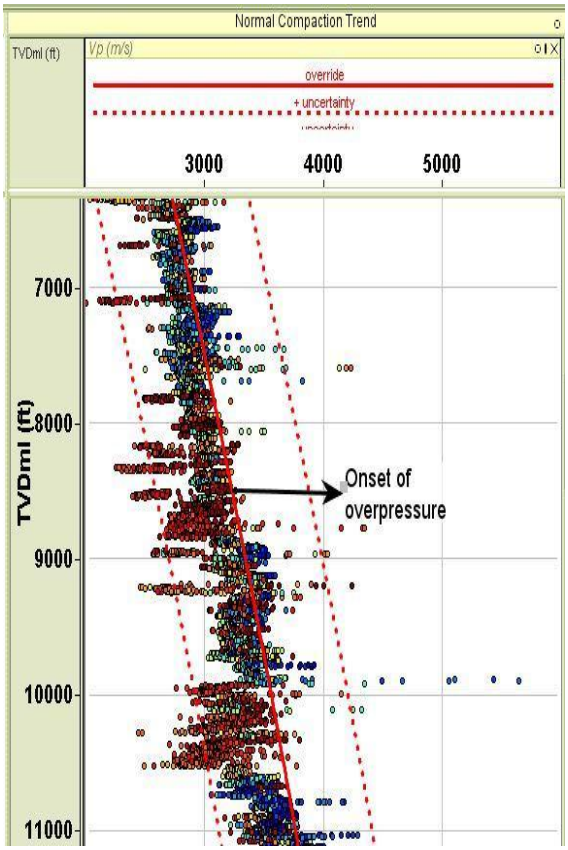

Showing Sonic Velocity Generated NCT, Well B

Figure 11: Showing sonic velocity generated NCT for Well B

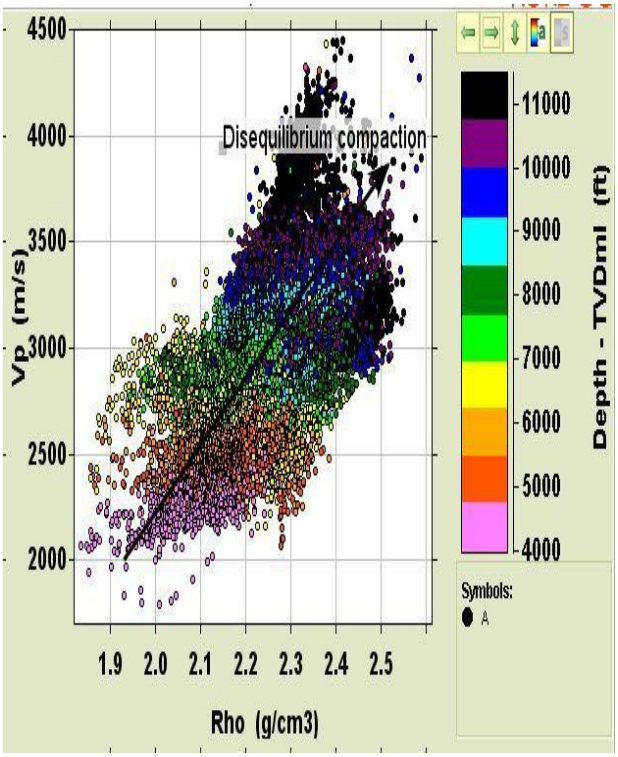

Figure 12: Vp – Rho crossplot (Coloured by depth) for Well A

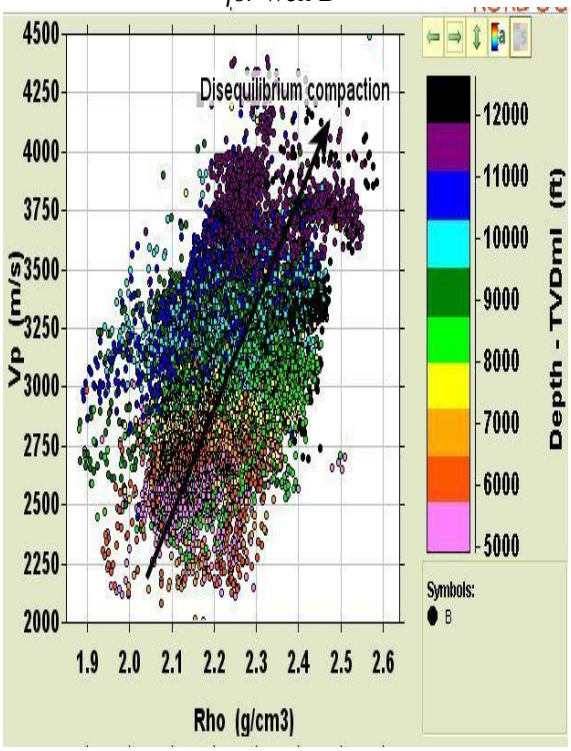

Figure 13: Vp - Rho Crossplot for Well B Coloured by Depth

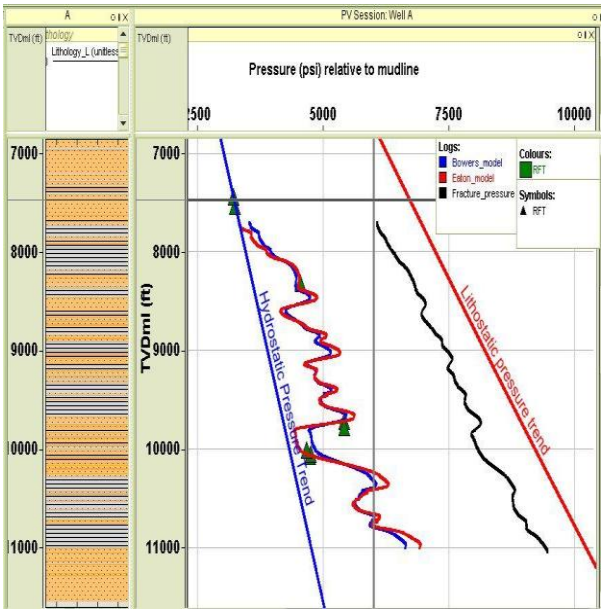

Figure 14: Pressure-Depth profile for Well A Final prediction

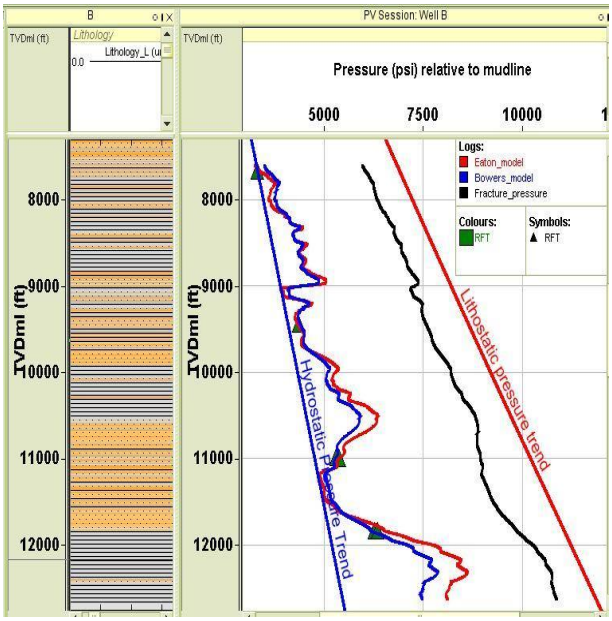

Figure 15: Pressure-Depth profile for Well B Final Prediction

Conclusion

Detailed fracture prediction in the study area revealed that onset overpressure was observed at about 770ft for both well A and B, overburden gradient ranges from 0.836psi/ft to about 0.934psi/ft for well A while for well B it ranges from 0.830psi/ft to about 0.928psi/ft. Prediction also showed that pressure gradient in wells A and B increased from hydrostatic Pressure gradient of about 0.433psi/ft to 0.6psi/ft indicating a mild overpresurring, while Fracture pressure prediction showed a fracture gradient from 0.790psi/ft for both wells.

The results of the present study would be useful in assessing seal effectiveness, mapping of hydrocarbon migration pathways, trap configuration, basin geometry, basin modelling, and safe and economic drilling. surface blowout, and underground blowout can be avoided by using an accurate estimation of pore pressure and fracture gradient.

Overpressures in Niger delta basin are as a result of compaction disequilibrium and secondary mechanism. The use of seismic method to predict pre-drill overpressure, will give a more accurate result.

Acknowledgement

The authors are indeed grateful to Shell Petroleum Development Company of Nigeria (SPDC) Port Harcourt Nigeria for aiding this study by prompt release of academic data for the purpose of this study.

References

[1]. Aigbedion, I., & Aigbedion, H.O. (2012). Hydrocarbon Volumetric Analysis using Seismic and Borehole data over Umoro field, Niger Delta-Nigeria. *International Journal of Geoscience*, 2:179 -183.

[2]. Ajaegwu, N.E., Odoh, B.I., Akpunonu, E.O., Odiadi, I.I. & Anakwuba E. K. (2012). Late Miocene to Early Pliocene Palynostratigraphy and Paleoenvironments of ANE-1 well, Eastern Niger Delta, Nigeria. *Journal of Minning and Geology*, 48(1):31 – 43.

[3]. Avbovbo, A.A. (1978). Tertiary Lithostratigraphy of Niger Delta. *American Association of Petroleum Geologists Bulletin*, 62, 295-300

[4]. Bowers, G. L. (1995). Pore pressure estimation from velocity data: Accounting for overpressure mechanisms besides undercompaction: *Society of petroleum Engineer Drilling and Completions*, 1-19.

[5]. Burst, J.F. (1969). Diagenesis of Gulf Coast clayed sediments and its possible relation to petroleum migration. *American Association of Petroleum Geologists Bulletin*, 68: 35-63.

[6]. Dutta, N. C. (2002). Geopressure prediction using seismic data: Current status and road ahead. *Geophysics*, 67: 2012-2014.
[7]. Eaton, B.A. (1975). The equation for geopressure prediction from well logs. *Society Petroleum*, 50-63.
[8]. Ekweozor, C. M. and Daukoru, E. M. (1984). Petroleum source bed evaluation of Tertiary Niger Delta. *American Association of Petroleum Geologists Bulletin*, 70, 48-55
[9]. Frankl, E. J. and Cordry, E. A. (1967). The Niger Delta oil Province: Recent development, onshore and offshore Mexico City. *Seventh world petroleum congress proceedings* 2: 195-209.
[10]. Fertl, W.H. (1976). Abnormal formation pressures: *Elsevier Scientific Publishing Company*, 382
[11]. Hansom, J., and Lee, M.K. (2005). Effects of hydrocarbon generation, basal heat flow and sediment compaction on overpressure development: a numerical study. *Petroleum Geosciences*, 11: 4-10
[12]. Hoesni, M.J. (2004). *Origins of overpressures in Malay basin and it influence on petroleum system. Ph.D. Thesis*, Durham University.
[13]. Horsfall, O.I., and Cookey, J.E. (2014). Overpressure prediction through porosity estimation in sedimentary formations using geophysical well logs in the Niger Delta basin of Nigeria.
[14]. Hunt, J.M. (1990). Generation and migration of petroleum from abnormally pressured fluid compartments: *American Association of Petroleum Geologists Bulletin*, 72: 1-12
[15]. Luo, M., and Vasseur, G., (1992). Contributions of compaction and aquathermal pressuring to geopressure and the influence of environmental conditions. *American Association of Petroleum Geologists Bulletin*, 76: 1550-1559
[16]. Matthews, W.R., Kelly, J. (1967). How to predict formation pressure and fracture gradient. *Oil and Gas Journal*, 780(65): 92-106.
[17]. Mouchet, J. P. & Mitchell A. F. (1989). Abnormal Pressures while drilling: Origins, prediction Detection, Elf Aquitaine Edition, Evaluation Techniques vol.2, pp.225
[18]. Nwozor, K.K., Omudu, M.L., Ozumba, B.M., Egbuachor, C.J., Onwuemesi, A.G., Anike, .L. (2013). Quantitative evidence of secondary mechanism of overpressure generation: Insight from parts of Onshore Niger Delta, Nigeria. *Petroleum technology development journal*, 3(1): 64-83.
[19]. Osborne, M.J., and Swarbrick, R.E. (1997). Mechanism for generating overpressure in sedimentary basins: A revaluation. *American Association of Petroleum Geologists Bulletin*, 81:1023-1041.
[20]. Petroconsultants. (1996). Petro World 21: Houston, Texas, Petroconsultants, Inc. (database available from Petroconsultants, Inc. P.O. Box 740619, Houston, TX 77274 -06191). Petroleum system, Niger Delta, Nigeria. In Magoon, L.B., & Dow, W.G., (eds.) The petroleum system from source to trap. *American Association of Petroleum Geologists Memoir*, 460:599-613.
[21]. Short, K.C., and Stauble, A.J. (1967). Outline of geology of Niger Delta: *American Association of Petroleum Geologists Bulletin*, 51:761-779.
[22]. Swarbrick, R. E. (2002). Challenges of Porosity-based pore pressure prediction: *CSEG Recorder*, 2: 4-8.
[23]. Terzaghi, K., (1943). *Theoretical soil mechanics*: John Wiley and Sons, Inc.
[24]. Tissot, B.P., Pelet, R., and Ungerer, P.H. (1987). Thermal history of sedimentary basins maturation indices and kinetics of oil and gas migration, *American Association of Petroleum Geologists Bulletin*, 71:1445-1466
[25]. Uko, E. D., Emudianughe, J. and Tamunobereton-ari, I. (2013). Overpressure prediction in the north-west Niger Delta using porosity data. *Journal of Applied Geology and Geophysics*, 1(3): 42-50.
[26]. Weber, K. J. and Daukoru, E. M. (1975), Petroleum Geological Aspects of the Niger Delta. *Proceedings of Ninth World Petroleum Congress, Tokyo*. 5(2): 209-221.
[27]. Zizhen Wang, Ruihe Wang. (2015) Pore pressure prediction using geophysical methods in carbonate reservoirs: Current status, challenges and way ahead. *Journal of Natural Gas Science and Engineering*, 27: 986-993.